Hindawi Publishing Corporation
EURASIP Journal on Wireless Communications and Networking
Volume 2009, Article ID 786040, 11 pages
doi:10.1155/2009/786040

Research Article

Intercarrier Interference in OFDM: A General Model for Transmissions in Mobile Environments with Imperfect Synchronization

Martín García and Christian Oberli

Department of Electrical Engineering, Pontificia Universidad Católica de Chile, 7820436 Macul, Santiago, Chile

Correspondence should be addressed to Christian Oberli, obe@ing.puc.cl

Received 2 June 2009; Accepted 16 September 2009

Recommended by Stefan Kaiser

Intercarrier Interference (ICI) is an impairment well known to degrade performance of Orthogonal Frequency Division Multiplexing (OFDM) transmissions. It arises from carrier frequency offsets (CFOs), from the Doppler spread due to channel time-variation and, to a lesser extent, from sampling frequency offsets (SFOs). Literature reports several models of ICI due to each kind of impairment. Some studies describe ICI due to two of the three impairments, but so far no general model exists to describe the joint effect of all three impairments together. Furthermore, most available models involve some level of approximation, and the diversity of approaches makes it cumbersome to compare power levels of the different kinds of ICI. In this work, we present a general and mathematically exact model for the ICI stemming from the joint effect of the three impairments mentioned. The model allows for a vis-a-vis comparison of signal-to-ICI ratios (SIRs) caused by each impairment. Our result was validated by simulations. An analysis of ICI in IEEE-802.16e-type transmissions shows that during steady-state tracking and at speeds below 150 km/h, SIR due to CFO is typically in the range between 25 dB and 35 dB, SIR due to Doppler spread is larger than 25 dB, and ICI due to SFO is negligible.

1. Introduction

Mathematical models of Intercarrier Interference (ICI) in Orthogonal Frequency Division Multiplexing (OFDM) and techniques for mitigating it have been reported by many authors. Studies modeling and dealing with ICI stemming individually from channel variation in time are [1–9]. Likewise, the works of [10–15] address ICI due to Carrier Frequency Offset (CFO) and those of [16, 17] ICI solely due to Sampling Frequency Offset (SFO). Work modeling ICI produced jointly by two of the three impairments is significantly less common. The joint effect of CFO and SFO has been studied in [18, 19], while [20] reports on ICI due to CFO and channel mobility. Despite the attention that the topic has received so far, there is as yet no general model in literature that describes ICI resulting from the joint effect of all three impairments.

Many of the above cited references model ICI by using discrete-time and discrete-frequency signals. Unfortunately, discrete-domain approaches are inaccurate for representing impairments that affect signals outside the time-frequency grid of discrete analysis, such as the SFO, or often restrict the time-frequency properties of the channels for which the approaches are valid. Another limitation of the models in the cited references is the difficulty of combining them in order to make a fair comparison of each kind of ICI under the same conditions.

Our contribution with this paper is the derivation of the general and mathematically exact model of ICI for OFDM transmissions subject to the joint effect of CFO, SFO, and time-varying channels with arbitrary statistics. By including continuous-domain analysis, our derivations yield a model that is general and is devoid of the limitations of purely discrete-domain approaches, and by modeling all three impairments together, we obtain a tool that allows for a direct and clear comparison of the ICI caused by each impairment.

The remainder of this work is organized as follows. Section 2 presents the development of our model of ICI with deterministic signals; Section 3 analyzes the statistical behavior of ICI; in Section 4, the statistical behavior predicted by our model is validated by simulations of IEEE-802.16e-type transmissions ("mobile WiMAX") [21]. Signal-to-interference ratio curves for a broad range of mobile speeds and CFOs are provided; finally, Section 5 sets out our conclusions.

2. Deterministic Model of ICI

In what follows, we derive a mathematical model that includes the effects of CFO, SFO, and channel mobility on OFDM transmissions.

We begin by modeling the signal of the mth OFDM symbol in continuous time t using complex baseband notation as

$$x(t) = \sqcap\left(\frac{t-(m+1/2)T_g+T_e}{T_g}\right) \cdot \sum_{\nu=-N_s/2}^{N_s/2-1} X_m(\nu)e^{j2\pi\nu(t-mT_g)\delta_t}. \tag{1}$$

In this equation, $X_m(\nu)$ is the modulation on subcarrier ν of a total of N_s subcarriers. The separation between subcarriers is $\delta_t = 1/N_sT$ Hertz, where T is the sampling period of the transmitter. The cyclic prefix has N_e samples and duration of $T_e = N_eT$ seconds. Thus, the complete OFM symbol has $N_g = N_e + N_s$ samples and duration of $T_g = N_gT$ seconds. The symbol j denotes the imaginary unit $\sqrt{-1}$. Finally, $\sqcap(x)$ is the rectangular function, equal to 1 when x is between $[-1/2, 1/2]$ and 0 elsewhere.

In [22, 23], the general input-output relationship of time-variant linear systems is described as

$$y(t) = \int_0^\infty h(t,\tau)x(t-\tau)d\tau, \tag{2}$$

where $x(t)$ and $y(t)$ are the respective input and output signals in the time domain. The function $h(t,\tau)$ is the time-variant impulse response of the system observed at instant t due to an impulse at time $t-\tau$.

Now consider $h(t,\tau)$ to represent the baseband-equivalent impulse response of a time-varying wireless channel, and substitute (1) for $x(t)$ in (2) to represent an OFDM transmission through that channel. At the receiver, the arriving (passband) signal becomes corrupted by Additive White Gaussian Noise (AWGN), is then downconverted to baseband with a CFO of Δf Hertz, and sampled with an SFO of ΔT seconds. Following the steps outlined in Appendix A for including these impairments, we obtain the following sampled received signal for the mth OFDM symbol:

$$\begin{aligned} y_s(t) = (T+\Delta T)\sum_{p=0}^{N_s-1}\sum_{\nu=-N_s/2}^{N_s/2-1} & X_m(\nu)e^{j2\pi\Delta f t}e^{-j2\pi\nu\delta_t mT_g} \\ & \cdot \delta\Big(t-p(T+\Delta T)-mN_g(T+\Delta T)\Big) \\ & \cdot \left[\int_0^\infty h(t,\tau)e^{j2\pi\nu\delta_t(t-\tau)} \right. \\ & \left. \cdot \sqcap\left(\frac{t-\Big((1/2)N_s+mN_g\Big)(T+\Delta T)}{N_s(T+\Delta T)}\right)d\tau\right] + n_s(t). \end{aligned} \tag{3}$$

Above, $\delta(\cdot)$ is the impulse function and $n_s(t)$ is AWGN sampled at instants $t = p(T+\Delta T) + mN_g(T+\Delta T)$, with $p = 0,\ldots,N_s-1$. Equation (3) is a continuous-time signal, but its value is 0 at every instant except when $t = p(T+\Delta T) + mN_g(T+\Delta T)$, with $p = 0,\ldots,N_s-1$.

To recover the symbols in an actual OFDM system implementation, the Fast Fourier Transform (FFT) of the N_s samples is calculated. That operation is equivalent to calculating the continuous Fourier transform of (3) with respect to t, but with the origin fixed at time $mN_g(T+\Delta T)$ (i.e., taking the transform of $y(t+mN_g(T+\Delta T))$). It is to be noted that we assume that the cumulative drift of the FFT window due to SFO has not yet reached the previous or following OFDM symbol. Intersymbol interference is therefore not considered in our model. Upon following the algebraic steps detailed in Appendix B, we obtain

$$\begin{aligned} Y_s(f) = \left(\int_0^\infty \left[s^{\sqcap}(f,\tau) *_f \left\{ (T+\Delta T)\sum_{\nu=-N_s/2}^{N_s/2-1} X_m(\nu) \right.\right.\right. & \\ \cdot e^{-j2\pi(f-\Delta f-\nu\delta_t)(T+\Delta T)(mN_g+(N_s-1)/2)} & \\ \cdot \frac{\sin[\pi(f-\Delta f-\nu\delta_t)(T+\Delta T)N_s]}{\sin[\pi(f-\Delta f-\nu\delta_t)(T+\Delta T)]} & \\ \left.\left.\left. \cdot e^{-j2\pi\nu\delta_t\tau}e^{-j2\pi\nu\delta_t mT_g}\right\}\right]d\tau\right)e^{j2\pi f mN_g(T+\Delta T)} & \\ + N_s(f). & \end{aligned} \tag{4}$$

In this equation the function $s^{\sqcap}(f,\tau)$ is the Doppler-variant impulse response [22], time-limited to the duration of the mth OFDM symbol. Thus, $s^{\sqcap}(f,\tau)$ is given by the Fourier Transform:

$$\begin{aligned} s^{\sqcap}(f,\tau) &= \mathcal{F}\left\{h(t,\tau)\sqcap\left(\frac{t-\Big((1/2)N_s+mN_g\Big)(T+\Delta T)}{N_s(T+\Delta T)}\right)\right\} \\ &= N_s(T+\Delta T)\mathrm{sinc}\big(fN_s(T+\Delta T)\big) \\ &\quad \cdot e^{-j2\pi f((1/2)N_s+mN_g)(T+\Delta T)} *_f s(f,\tau), \end{aligned} \tag{5}$$

where $s(f,\tau)$ is the Doppler-variant impulse response defined as the Fourier transform in t of $h(t,\tau)$ [22]. For a fixed delay τ, and if the channel is static, then $s(f,\tau)$ is a frequency domain impulse. As channel mobility increases, so does the frequency spread of $s(f,\tau)$. The symbol $*_f$ denotes continuous convolution in the frequency domain.

Expression (4) gives an exact description of the continuous spectrum of an OFDM signal received over a time-variant channel with a CFO of Δf Hertz and an SFO of ΔT seconds. In practice, this signal is observed at the output of the FFT in the receiver at frequencies of $f = l\delta_r$, with $-N_s/2 \le l \le N_s/2 - 1$ and $\delta_r = 1/N_s(T + \Delta T)$ being equal to the separation of the subcarrier frequencies used by the receiver. Imposing these conditions on (4) and considering an arbitrary subcarrier k, we obtain (Appendix C) the discrete output of the system:

$$Y(k) = \beta(k,k)\overline{H}(k)X_m(k) + I(k) + W(k) + Q(k) + N(k), \tag{6}$$

where $\beta(\cdot,\cdot)$ is a phase and magnitude distortion given by

$$\begin{aligned}\beta(d,\nu) &= \frac{1}{N_s} e^{j2\pi(d-\nu)\delta_t m T_g} \\ &\cdot e^{-j2\pi\left[(d-\nu)/N_s - (\nu/N_s)(\Delta T/T) - \Delta f T(1+\Delta T/T)\right](mN_g + (N_s-1)/2)} \\ &\cdot \frac{\sin\{\pi[(d-\nu)/N_s - (\nu/N_s)(\Delta T/T) - \Delta f T(1+\Delta T/T)]N_s\}}{\sin\{\pi[(d-\nu)/N_s - (\nu/N_s)(\Delta T/T) - \Delta f T(1+\Delta T/T)]\}},\end{aligned} \tag{7}$$

and $\overline{H}(k)$ in (6) is the time domain average of the channel in carrier k during the transmission of the mth OFDM symbol, given by

$$\begin{aligned}\overline{H}(k) &= \frac{1}{N_s(T+\Delta T)} \cdot \int_0^\infty s^{\sqcap}(0,\tau) e^{-j2\pi k\delta_t\tau} d\tau \\ &= \int_0^\infty \frac{e^{-j2\pi k\delta_t\tau}}{N_s(T+\Delta T)} \int_{mN_g(T+\Delta T)}^{(N_s+mN_g)(T+\Delta T)} h(t,\tau)\, dt\, d\tau.\end{aligned} \tag{8}$$

Finally $I(k)$, $W(k)$, and $Q(k)$ in (6) represent various forms of intercarrier interference (ICI). Concretely, $I(k)$ is ICI due solely to mobility, $W(k)$ is ICI caused exclusively by imperfect synchronization, and $Q(k)$ is an ICI that is nonzero only when both impairments are present. Their expressions are

$$\begin{aligned}I(k) = \frac{1}{N_s(T+\Delta T)} &\sum_{\substack{d=-N_s/2 \\ d\neq k}}^{N_s/2-1} X_m(d)\beta(d,d) \\ &\cdot \int_0^\infty s^{\sqcap}((k-d)\delta_r,\tau) e^{-j2\pi d\delta_t\tau} d\tau,\end{aligned} \tag{9}$$

$$W(k) = \sum_{\substack{\nu=-N_s/2 \\ \nu\neq k}}^{N_s/2-1} X_m(\nu)\beta(k,\nu)\overline{H}(\nu), \tag{10}$$

$$\begin{aligned}Q(k) = \frac{1}{N_s(T+\Delta T)} &\sum_{\substack{d=-N_s/2 \\ d\neq k}}^{N_s/2-1} \sum_{\substack{\nu=-N_s/2 \\ \nu\neq d}}^{N_s/2-1} X_m(\nu)\beta(d,\nu) \\ &\cdot \int_0^\infty s^{\sqcap}((k-d)\delta_r,\tau) e^{-j2\pi\nu\delta_t\tau} d\tau.\end{aligned} \tag{11}$$

Results (6) through (11) are deterministic and mathematically exact. In (9) (ICI due to mobility) we observe that the interference in subcarrier k is the sum of signals from all the other subcarriers, respectively weighted by the integral of $s^{\sqcap}((k-d)\delta_r,\tau)$. The value of the integral depends on mobility and on the separation between the interfering subcarriers (d) and the desired subcarrier (k). This value is relevant only when subcarrier d is in the neighborhood of k. The size of the neighborhood grows with the mobile's speed, but in any current-day OFDM systems designed for mobility (e.g., DVB-T/H [24], "mobile WiMAX" [21]), the neighborhood is mainly comprised by subcarriers $k+1$ and $k-1$. It is to be noted that (9) equals zero if the channel is static, regardless of synchronization. If synchronization is perfect (i.e., $\Delta T = 0$ and $\Delta f = 0$), then (9) is similar to the description found by many authors [2, 6, 9, 25] for representing interference based on Doppler-variant impulse responses. However, they all use discrete-domain approaches, different from the one employed here, thus capturing the effect of ICI less accurately.

Term (10) (ICI due to imperfect synchronization) has been described by several authors for static channel conditions, either considering CFO and SFO jointly [18, 19], CFO alone [10, 12], or SFO alone [16, 17]. This term equals zero if and only if there are no frequency nor sampling offsets, regardless of mobility.

Finally, $Q(k)$ of (11) is a new finding and clarifies a frequent misconception that ICI due to mobility and imperfect synchronization is two separate additive terms. There is an ICI enhancement when both impairments are jointly present (we will show in Section 4, however, that this ICI is negligible in practice).

3. Statistical Analysis of ICI

In this section we analyze the statistical properties of ICI on the basis of the expressions derived in the previous section. The analysis that follows assumes a WSSUS (wide-sense

stationary with uncorrelated scattering) channel [22, 23], meaning that

$$\mathrm{E}\{s(f_1,\tau_1)s^*(f_2,\tau_2)\} = \delta(f_2-f_1)\delta(\tau_2-\tau_1)S_{ss}(f_1,\tau_1), \tag{12}$$

where $S_{ss}(f,\tau)$ is the scattering function [22, 23]. It is also assumed that the transmitted data symbols are not correlated either in frequency or in time and have an average energy of E_s.

The relationship between the Doppler power spectral density and the scattering function is [23]

$$S(f) = \int_0^\infty S_{ss}(f,\tau)\,d\tau, \tag{13}$$

where $S(f)$ is the power spectral density of a pure tone received under conditions of mobility. Perhaps the most widely used model for this density is the one due to Clarke [26] (often referred to as Jakes' Doppler spectrum):

$$S(f) = \begin{cases} \dfrac{1}{\pi f_D\sqrt{1-(f/f_D)^2}}, & \text{if } |f| \le f_D, \\ 0, & \text{if } |f| > f_D, \end{cases} \tag{14}$$

where f_D is the maximum Doppler spread as given by $f_D = v/\lambda$, with v denoting the mobile's speed and λ the carrier wavelength.

We define the function $S^{\sqcap}(f)$ as the Doppler power density of the baseband-equivalent of a time-limited carrier wave, that is, the Doppler density $S(f)$ convoluted in frequency with a $\mathrm{sinc}^2(\cdot)$ function:

$$S^{\sqcap}(f) = \mathrm{sinc}^2\left(fN_s(T+\Delta T)\right) *_f S(f). \tag{15}$$

Based on the foregoing considerations, we show in Appendix D that the expected power of ICI on subcarrier k is composed by three additive terms as

$$\begin{aligned} &\mathrm{E}\left\{|I(k)+W(k)+Q(k)|^2\right\} \\ &\quad = \mathrm{E}\left\{|I(k)|^2\right\} + \mathrm{E}\left\{|W(k)|^2\right\} + \mathrm{E}\left\{|Q(k)|^2\right\} \\ &\quad = S_I(k) + S_W(k) + S_Q(k), \end{aligned} \tag{16}$$

where the notation used is self-evident. The three power terms are, respectively, given by

$$S_I(k) = E_s \sum_{\substack{d=-N_s/2 \\ d\neq k}}^{N_s/2-1} \beta(d,d)\beta^*(d,d)S^{\sqcap}((k-d)\delta_r), \tag{17}$$

$$S_W(k) = E_s \sum_{\substack{\nu=-N_s/2 \\ \nu\neq k}}^{N_s/2-1} \beta(k,\nu)\beta^*(k,\nu)S^{\sqcap}(0), \tag{18}$$

$$S_Q(k) = E_s \sum_{\substack{d=-N_s/2 \\ d\neq k}}^{N_s/2-1} \sum_{\substack{\nu=-N_s/2 \\ \nu\neq d}}^{N_s/2-1} \beta(d,\nu)\beta^*(d,\nu)S^{\sqcap}((k-d)\delta_r). \tag{19}$$

Note that (16) implicitly states that the three ICI terms are statistically independent from each other.

In [27], the steps of Appendix D were also followed for determining the covariances of the ICI terms between different subcarriers. The result can be used for generating statistically accurate frequency-correlated ICI from a white Gaussian sequence. (By virtue of the central limit theorem with N_s large enough it is commonly accepted that ICI has Gaussian random properties; see, e.g., [25].) The ICI thus generated might greatly simplify some simulations of imperfectly synchronized OFDM systems in mobile environments.

Finally, using (6) and (8) (and WSSUS conditions), we can calculate the expected power of the desired symbol actually received on subcarrier k:

$$\begin{aligned} S_X(k) &= \mathrm{E}\left\{\beta(k,k)X(k)\overline{H}(k)\ \beta^*(k,k)X(k)^*\overline{H}^*(k)\right\} \\ &= E_s\cdot\beta(k,k)\beta^*(k,k)S^{\sqcap}(0), \end{aligned} \tag{20}$$

where $\mathrm{E}[\overline{H}(k)\overline{H}^*(k)] = S^{\sqcap}(0)$ follows from (8) and (15).

Strictly speaking, the expected interference powers per subcarrier given by (17), (18), (19), and (20) change with k. In practice, however, if the transmission bandwidth is much larger than the Doppler spread bandwidth, these terms are practically constant over frequency. This is so because the time-limited Doppler spread function ($S^{\sqcap}(f)$) takes significant values only in the neighborhood of a subcarrier k, thus ensuring statistical homogeneity in most subcarriers other than those at the band edges, which are exposed to less ICI because they have fewer neighboring subcarriers.

We define $\eta = S_X(k)/E_s$ as the fraction of energy kept by subcarrier k. If we assume perfect synchronization then by (20) we can calculate η as a measure of degradation due only to channel mobility. Using (14) and (15), we obtain the precise value of η as follows:

$$\eta = \int_{-v/\lambda}^{v/\lambda} \frac{\lambda\,\mathrm{sinc}\left(fN_sT\right)^2}{\pi v\sqrt{1-(\lambda f/v)^2}}\,df. \tag{21}$$

An example of (21) is shown in Figure 1(a) for a IEEE-802.16e transmission with 512 subcarriers ("mobile WiMAX") [21]. At speeds under 500 km/h, the subcarrier energy retention is over 95%.

A similar performance measure can be calculated for a case without mobility but with imperfect synchronization. Using (20) and (7) and considering $(v/N_s)(\Delta T/T) \approx 0$, we obtain

$$\eta = \frac{1}{N_s^2}\frac{\sin^2\{\pi[\Delta f T(1+\Delta T/T)]N_s\}}{\sin^2\{\pi[\Delta f T(1+\Delta T/T)]\}}. \tag{22}$$

In this case, the WiMAX system requires a CFO smaller than 0.2 intercarrier spacing so that less than 10% of energy is lost as ICI (Figure 1(b)).

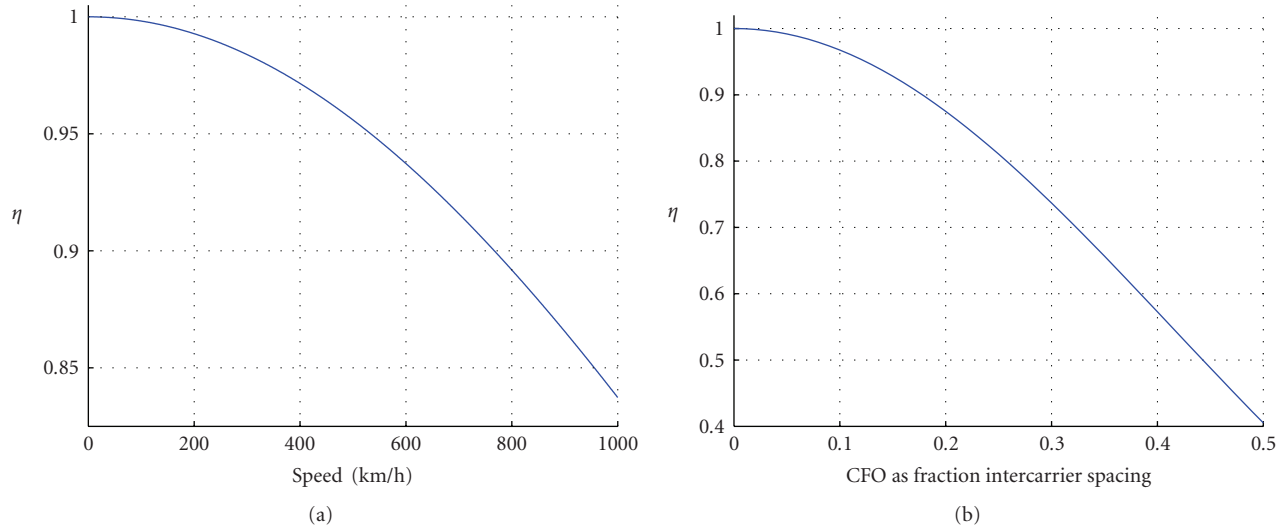

Figure 1: Fraction of energy retained by a subcarrier as (a) mobile's speed increases and (b) as carrier frequency offset increases. The remaining energy is lost as intercarrier interference. System parameters: 512 subcarriers, 5 MHz bandwidth, 3.5 GHz carrier frequency.

4. Computational Verification of Results

We now turn to the computational validation of (17), (18), (19), and (20) found in Section 3. For this, consider defining the signal-to-interference-plus-noise ratio (SINR) of a subcarrier k as

$$\mathrm{SINR}(k) = \frac{S_X(k)}{S_I(k) + S_W(k) + S_Q(k) + E_s/\Gamma}. \tag{23}$$

Above, the parameter Γ is defined such that transmissions have an expected signal-to-noise ratio (SNR) of Γ when there is no ICI (i.e., no mobility and perfect synchronization, hence (23) evaluates to Γ).

Our goal is to compare the theoretical prediction of (23) with values of SINR obtained from simulations by averaging over 300 OFDM symbols, transmitted over the same number of independent realizations of WSSUS time-varying channels with Clarke's statistics, and with receiver-side insertion of CFO and SFO. The time-variant impulse responses $h(t, \tau)$ were generated using an autoregressive model of order 100 as set out in [28], with an $\epsilon = 10^{-5}$ bias to ensure the algorithm's stability. Unit-power QPSK was used for subcarrier modulation.

The parameters used were those of an IEEE-802.16e system [21] with $N_s = 512$ subcarriers, a cyclic prefix of $N_e = 64$, bandwidth of 5 MHz, and a carrier of 3.5 GHz. Finally, the coherence time was estimated as $T_c = 0.423/f_D$ [29], the average symbol energy E_s was set equal to 1, and the channels' maximum delay spread was restricted to the duration of the cyclic prefix.

Note that evaluating (17), (18), (19), and (20) for (23) requires computing continuous integrals given by (8) and (15) (the latter was computed based on (14)). These were carried out with a sampling density of 100 points between subcarriers. In order to reduce the computational complexity of the resulting calculations, we used the fact that (17) to (20) are essentially invariant in k (as noted) and therefore confined ourselves for evaluating the case of $k = 0$.

A first set of simulations illustrates the individual contributions of CFO, SFO, and environment mobility to the signal-to-interference ratio (SIR) in the absence of thermal noise (Figure 2). Solid curves show evaluations of (23) and markers quantify simulation results. Curve A shows the SIR due only to mobility (S_X/S_I) when synchronization is ideal. For cases with imperfect synchronization, note that the SIR S_X/S_W is a constant with respect to the channel's coherence time. The SIR is thus shown by asymptotes B1 for the case with CFO = 0.2 parts of one intercarrier spacing and SFO = 0 ppm, and C1 for the case with CFO = 0 and SFO = 20 ppm. Correspondingly, curves B2 and C2 present the ratios $S_X/(S_W + S_Q)$. They confirm that S_Q is relevant only in transmissions with extremely high mobility and has no practical relevance in current-day OFDM systems. Similarly, the contribution of SFO to SIR (curves C1 and C2) is also negligible compared to the effect of mobility and CFO, even with the rather large SFO used here.

We now focus on the simulation results for SINR with different CFOs and coherence times. Figures 3 and 4 display some of these results for $\Gamma = 7$ dB and $\Gamma = 12$ dB. Observe that for high-mobility channels, where coherence times are less than approximately 3 OFDM symbols, SINR degrades dramatically, regardless of the magnitude of CFO. This implies that for the range of coherence times just indicated, CFO-induced degradation is overshadowed by the degradation due to mobility. By contrast, with greater coherence times, the ICI produced by CFO tends to dominate the SINR. A graphic representation of how SINR varies with CFO for different levels of thermal noise is presented in Figure 5. It shows that taking full advantage of OFDM performance in high SNR regimes needs tighter synchronization requirements than at lower SNRs.

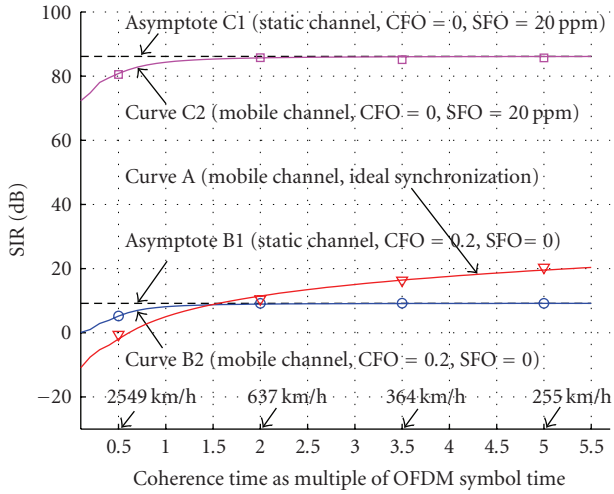

Figure 2: Individual contributions of mobility (curve A), carrier frequency offset (CFO, curves B1 and B2), and sampling frequency offset (SFO, curves C1 and C2) to the SIR. Solid curves are evaluations of (23) and markers represent simulation results. System parameters are as in Figure 1.

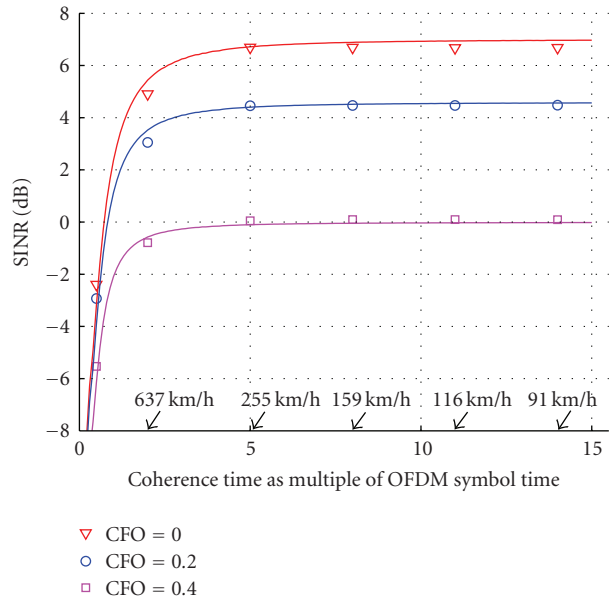

Figure 3: SINR for different carrier frequency offset as a function of channel coherence time. Solid curves are evaluations of (23) and markers represent simulation results. System parameters are as in Figure 1, SNR $\Gamma = 7$ dB.

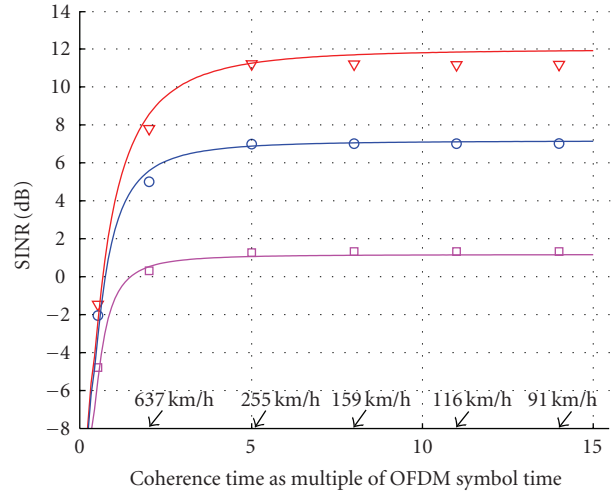

Figure 4: SINR as in Figure 3 with $\Gamma = 12$ dB.

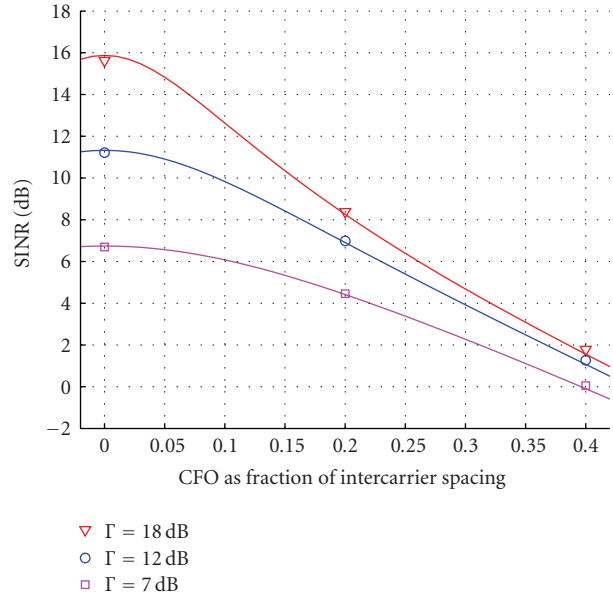

Figure 5: SINR as a function of carrier frequency offset for SNR levels $\Gamma = \{7, 12, 18\}$ dB. Channel coherence time is 5 OFDM symbols. Solid curves are evaluations of (23) and markers represent simulation results. System parameters are as in Figure 1.

The top curves of Figures 3 and 4 present a discrepancy between theoretical and simulation results. As discussed by Baddour and Beaulieu [28], the autoregressive approach for simulating a time-varying channel uses ill-conditioned equations, which makes simulating slow-varying channels with Clarke's U-shaped spectral density difficult. As a workaround, they propose a heuristic solution equivalent to adding a very small amount of white noise to the channel's fading process. The effect is also equivalent to a slight enhancement of thermal noise and reveals itself in our simulations when thermal noise dominates over ICI, as in the curves mentioned. When this simulation bias is negligible, however, our theoretical results are well matched by the simulations.

The values used above for CFO (0.2 and 0.4) are adequate for representing initial conditions of tracking loops after an acquisition stage. But during steady-state tracking, typical RMS values of the residual CFO are in the range between

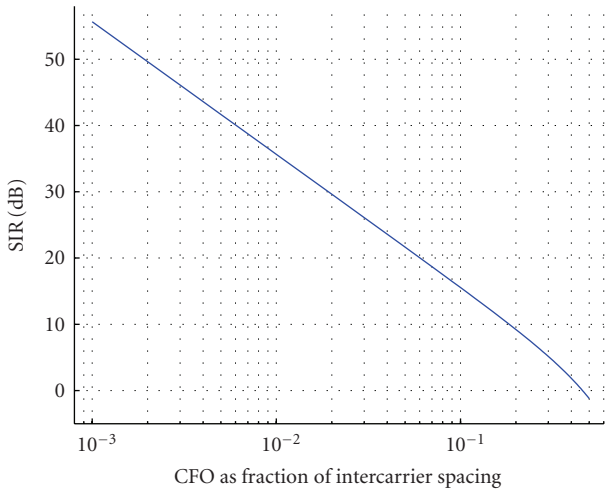

Figure 6: SIR as a function of carrier frequency offset (CFO). Obtained from (23) with static channel, SNR $\Gamma = \infty$ and system parameters are as in Figure 1.

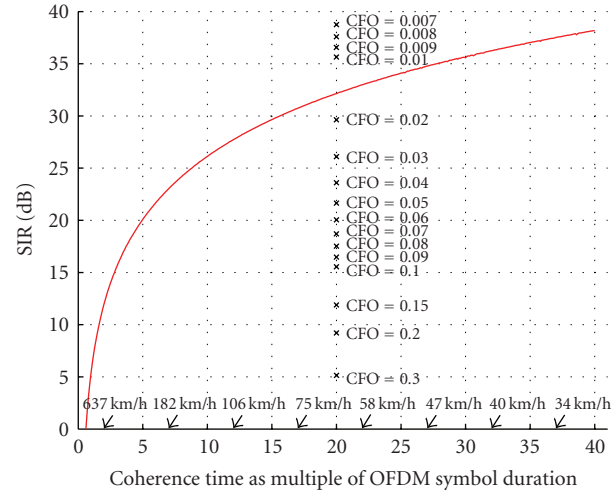

Figure 7: SIR as function of mobility. Obtained from (23) with no carrier frequency offset (CFO), SNR $\Gamma = \infty$ and system parameters are as in Figure 1. Selected SIR levels due to CFO are also given for comparison ($\times$-markers, values copied over from Figure 6).

0.01 ($\Gamma = 18$ dB) and 0.04 ($\Gamma = 7$ dB) [19]. Because of the algorithmic limitations discussed above, simulating these cases of CFO for channels with coherence times of practical interest yields inaccurate results. However, we can now predict precise SIR levels by evaluating (23). Figure 6 shows the SIR due only to CFO for a broad range of CFO values. The surprising linearity of the relationship between SIR and CFO is not at all evident from the equations. For the residual CFOs given before, SIR is in the range between 25 dB and 35 dB. In similar fashion, Figure 7 presents the SIR for a wide range of mobile speeds. For mobile speeds below 150 km/h, SIR is larger than 25 dB. Observe that Figures 6 and 7, used along with an SNR level Γ, provide a quick way for ranking the three impairments in terms of their contribution to SINR and for determining link-level SINR values without having to resort to time-consuming simulations.

Finally, note that after neglecting SFO the sole parameter remaining in (17), (18), (19), and (20) is the intercarrier spacing $1/N_sT = 1/T_s$. Because all modes of operation specified by the IEEE-802.16e standard use the same intercarrier spacing [21], it follows that the curves in Figures 2 through 7 are in fact valid for any mode of mobile WiMAX transmission.

5. Conclusions

A general and mathematically exact model of the power of intercarrier interference (ICI) was derived for OFDM transmissions exposed to the joint impact of sampling frequency offset, carrier frequency offset (CFO), and channel time variation. It was shown that the ICI ensuing from these impairments has three components: one solely caused by Doppler spread, one that depends only on the synchronization offsets, and one that is nonzero only when imperfect synchronization and channel variation happen together. Similar but nevertheless approximate descriptions of the former two components are available in literature. In this paper, besides describing them without approximations, they are presented with the same power scale. This allows for a direct comparison of these two sources of ICI. The third component is a new finding. It was shown to be nonnegligible only in very-high-speed environments of no practical interest at the present.

The new model was validated by computer simulations of OFDM transmissions using IEEE 802.16e parameters (mobile WiMAX).

Signal-to-noise and signal-to-interference ratios (SIR) were used for comparing the different sources of ICI with levels of thermal noise. SIR curves for a broad range of CFOs and mobile speeds were presented. For reference, during steady-state tracking and at speeds below 150 km/h, SIR due to carrier frequency offset is typically in the range between 25 dB and 35 dB, and ICI due to Doppler spread is larger than 25 dB.

Appendices

A. Sampled Received Signal

By substituting (1) into (2) and adding the phasor $e^{j2\pi\Delta ft}$ due to the difference of Δf Hertz between the receiver and transmitter carrier frequencies, we obtain

$$y(t) = e^{j2\pi\Delta ft}\int_0^\infty \sqcap\left(\frac{t-\tau-(m+1/2)T_g+T_e}{T_g}\right) \cdot \sum_{\nu=-N_s/2}^{N_s/2-1} X_m(\nu)e^{j2\pi\nu\delta_t(t-\tau-mT_g)}h(t,\tau)d\tau + n(t). \tag{A.1}$$

We now sample the received signal (A.1) at a rate offset by ΔT seconds from the transmitter rate, that is, at instants $n\cdot(T+\Delta T)$, where T is the transmitter sampling period. If we assume that adequate filtering of the signal was conducted

prior to sampling so that the noise term $n(t)$ is limited to the band of interest, the sampling times for the mth OFDM symbol are $t = n(T + \Delta T) + mN_g(T + \Delta T)$, where $n = 0, \ldots, N_s - 1$. Thus, the sampling operation implicitly removes the cyclic prefix and extracts the OFDM symbol in the "correct" window except for a cumulative drift due to ΔT. The sampling function shah$(\cdot)$ representing this operation is given by

$$\begin{aligned}\operatorname{shah}\left(\frac{t}{T+\Delta T}\right) &= (T+\Delta T)\sqcap\left(\frac{t-\left((1/2)N_s+mN_g\right)(T+\Delta T)}{N_s(T+\Delta T)}\right)\\ &\cdot\sum_{p=-\infty}^{\infty}\delta\left(t-p(T+\Delta T)-mN_g(T+\Delta T)\right),\end{aligned} \tag{A.2}$$

where $\delta(\cdot)$ is the Dirac delta function. The scaling factor $T + \Delta T$ indicates sampling by area. This formulation of the sampling function, instead of simply representing it by a sum of N_s terms, is more convenient for the derivation in Appendix B leading to (4). Applying (A.2) to (A.1) we obtain

$$\begin{aligned}y_s(t) = &\sum_{p=-\infty}^{\infty}\delta\left(t-p(T+\Delta T)-mN_g(T+\Delta T)\right)\\ &\cdot(T+\Delta T)\sum_{\nu=-N_s/2}^{N_s/2-1}X_m(\nu)e^{j2\pi\Delta f t}\\ &\cdot\underbrace{\sqcap\left(\frac{t-\left((1/2)N_s+mN_g\right)(T+\Delta T)}{N_s(T+\Delta T)}\right)}_{\sqcap(\clubsuit)}\\ &\cdot\int_0^{\infty}\underbrace{\sqcap\left(\frac{t-\tau-(m+1/2)T_g+T_e}{T_g}\right)}_{\sqcap(\spadesuit)}h(t,\tau)\\ &\cdot e^{j2\pi\nu\delta_t(t-\tau-mT_g)}d\tau+\underbrace{\operatorname{shah}\left(\frac{t}{T+\Delta T}\right)\cdot n(t)}_{n_s(t)},\end{aligned} \tag{A.3}$$

where $mN_g(T + \Delta T) \le t \le (mN_g + N_s - 1)(T + \Delta T)$. If the cyclic prefix duration is sufficiently large that $h(t, \tau) \equiv 0$ for all $\tau > T_e$ at every instant t, a careful analysis of (A.3) will show that the presence of $\sqcap(\clubsuit)$ allows $\sqcap(\spadesuit)$ to be eliminated. This is so due to the condition on T_e and the position of the $\sqcap(\cdot)$ functions when m and ΔT are within the range of interest. Further simplification may be achieved by joining $\sqcap(\clubsuit)$ with the series in p, as given in (3).

B. Spectrum of Sampled Received Signal

If we calculate the transform of $y_s(t)$ in (3), evaluated at $t + mN_g(T + \Delta T)$, we obtain

$$\begin{aligned}Y_s(f) = &\int_0^{\infty}\underbrace{\int_{-\infty}^{\infty}\sqcap(\clubsuit)h(t,\tau)\psi(t,\tau)e^{-j2\pi ft}dt}_{\mathcal{F}_t\{\sqcap(\clubsuit)h(t,\tau)\psi(t,\tau)\}}d\tau\\ &\cdot e^{j2\pi fmN_g(T+\Delta T)}+N(f),\end{aligned} \tag{B.1}$$

where the function $\psi(t, \tau)$ is defined as

$$\begin{aligned}\psi(t,\tau) = &(T+\Delta T)\sum_{p=0}^{N_s-1}\sum_{\nu=-N_s/2}^{N_s/2-1}X_m(\nu)\\ &\cdot\delta\left(t-p(T+\Delta T)-mN_g(T+\Delta T)\right)\\ &\cdot e^{j2\pi\Delta f t}e^{-j2\pi\nu\delta_t mT_g}e^{j2\pi\nu\delta_t(t-\tau)}.\end{aligned} \tag{B.2}$$

In (B.1), $\mathcal{F}_t\{\cdot\}$ is the Fourier transform in t of the product $\sqcap(\clubsuit)h(t, \tau)\psi(t, \tau)$ for delay τ in the time-variant impulse response. The transform is given by

$$\mathcal{F}_t\{\sqcap(\clubsuit)h(t,\tau)\psi(t,\tau)\} = s^{\sqcap}(f,\tau)*_f\Psi(f,\tau), \tag{B.3}$$

where $s^{\sqcap}(f, \tau)$ and $\Psi(f, \tau)$ are the Fourier transforms in t of $\sqcap(\clubsuit)h(t, \tau)$ and $\psi(t, \tau)$, respectively, given by

$$s^{\sqcap}(f,\tau) = \int_{mN_g(T+\Delta T)}^{(N_s+mN_g)(T+\Delta T)}h(t,\tau)e^{-j2\pi ft}dt, \tag{B.4}$$

$$\begin{aligned}\Psi(f,\tau) = &(T+\Delta T)\sum_{\nu=-N_s/2}^{N_s/2-1}X_m(\nu)e^{-j2\pi\nu\delta_t mT_g}e^{-j2\pi\nu\delta_t\tau}\\ &\cdot e^{-j2\pi(f-\Delta f-\nu\delta_t)mN_g(T+\Delta T)}\\ &\cdot\sum_{p=0}^{N_s-1}e^{-j2\pi(f-\Delta f-\nu\delta_t)p(T+\Delta T)}.\end{aligned} \tag{B.5}$$

The last step is to directly evaluate the geometric series in (B.5), following [19]. We are then left with

$$\begin{aligned}\Psi(f,\tau) = &(T+\Delta T)\sum_{\nu=-N_s/2}^{N_s/2-1}X_m(\nu)e^{-j2\pi\nu\delta_t mT_g}e^{-j2\pi\nu\delta_t\tau}\\ &\cdot e^{-j2\pi(f-\Delta f-\nu\delta_t)(T+\Delta T)(mN_g+(N_s-1)/2)}\\ &\cdot\frac{\sin[\pi(f-\Delta f-\nu\delta_t)(T+\Delta T)N_s]}{\sin[\pi(f-\Delta f-\nu\delta_t)(T+\Delta T)]},\end{aligned} \tag{B.6}$$

which is the expression in curly brackets in (4). Substituting (B.4) and (B.6) into (B.1) and (B.3), we obtain the desired signal model in (4).

C. Received Subcarrier Signal

We first evaluate portions of (4) at the desired discrete frequencies $f = l\delta_r$, with $-N_s/2 \le l \le N_s/2 - 1$ and $\delta_r = 1/N_s(T + \Delta T)$ and find

$$e^{-j2\pi\nu\delta_t mT_g} e^{j2\pi f mN_g(T+\Delta T)} = e^{j2\pi(l-\nu)\delta_t mT_g},$$
$$(f - \Delta f - \nu\delta_t)(T + \Delta T) = \frac{l-\nu}{N_s} - \Delta f T\left(1 + \frac{\Delta T}{T}\right) - \frac{\nu}{N_s}\frac{\Delta T}{T}. \tag{C.1}$$

Also, the frequency-convolution integral in (4) becomes a summation (in d, below) with its differential df turning into $\delta_r = 1/N_s(T + \Delta T)$. The term $s^{\sqcap}(l\delta_r, \tau)$ is evaluated at the discrete frequencies l, with sample separation $\delta_r = 1/N_s(T+\Delta T)$, and to conserve energy it must be multiplied by δ_r. Thus, sampling (4) at frequency $l = k$ gives the following result:

$$\begin{aligned} Y(k) &= \frac{1}{N_s^2(T + \Delta T)} \sum_{d=-N_s/2}^{N_s/2-1} \sum_{\nu=-N_s/2}^{N_s/2-1} X_m(\nu) \\ &\cdot e^{j2\pi(d-\nu)\delta_t mT_g} \\ &\cdot e^{-j2\pi[(d-\nu)/N_s - (\nu/N_s)(\Delta T/T) - \Delta f T(1+\Delta T/T)](mN_g + (N_s-1)/2)} \\ &\cdot \frac{\sin\{\pi[(d-\nu)/N_s - (\nu/N_s)(\Delta T/T) - \Delta f T(1 + \Delta T/T)]N_s\}}{\sin\{\pi[(d-\nu)/N_s - (\nu/N_s)(\Delta T/T) - \Delta f T(1 + \Delta T/T)]\}} \\ &\cdot \int_0^\infty s^{\sqcap}((k-d)\delta_r, \tau) e^{-j2\pi\nu\delta_t\tau} d\tau + N(k). \end{aligned} \tag{C.2}$$

If we now separate out $\nu = d$ from the rest of the terms in the second summation of (C.2), we obtain

$$\begin{aligned} Y(k) = {} & \frac{1}{N_s(T + \Delta T)} \sum_{d=-N_s/2}^{N_s/2-1} X_m(d)\beta(d,d) \\ & \cdot \int_0^\infty s^{\sqcap}((k-d)\delta_r, \tau) e^{-j2\pi d\delta_t\tau} d\tau \\ & + \frac{1}{N_s(T + \Delta T)} \sum_{d=-N_s/2}^{N_s/2-1} \sum_{\substack{\nu=-N_s/2 \\ \nu\neq d}}^{N_s/2-1} X_m(\nu)\beta(d,\nu) \\ & \cdot \int_0^\infty s^{\sqcap}((k-d)\delta_r, \tau) e^{-j2\pi\nu\delta_t\tau} d\tau + N(k), \end{aligned} \tag{C.3}$$

in which $\beta(d, \nu)$ represents the phase and magnitude effects. This function is given in (7).

Finally, by isolating the terms $d = k$ from both sums on d in (C.3) and by using the definition of the time-domain average channel given in (8), we obtain (6), (9), (10), and (11).

D. Expected Power of ICI

For simplicity, we write $W(k)$ and $Q(k)$ as one term $\varphi(k) = W(k) + Q(k)$. Then, we have

$$\begin{aligned} &\mathrm{E}\left[(I(k) + \varphi(k))(I(k) + \varphi(k))^*\right] \\ &\quad = \mathrm{E}[I(k)I^*(k)] + \mathrm{E}[I(k)\varphi^*(k)] + \mathrm{E}[\varphi(k)I^*(k)] \\ &\qquad + \mathrm{E}[\varphi(k)\varphi^*(k)]. \end{aligned} \tag{D.1}$$

We now proceed term by term:

$$\begin{aligned} &\mathrm{E}[I(k)I^*(k)] \\ &\quad = \frac{1}{N_s^2(T + \Delta T)^2} \sum_{\substack{d_1=-N_s/2 \\ d_1\neq k}}^{N_s/2-1} \sum_{\substack{d_1=-N_s/2 \\ d_1\neq k}}^{N_s/2-1} \mathrm{E}[X_m(d_1)X_m^*(d_2)] \\ &\qquad \cdot \beta(d_1, d_1)\beta^*(d_2, d_2) \\ &\qquad \cdot \iint_0^\infty \mathrm{E}\left[s^{\sqcap}((k-d_1)\delta_r, \tau_1) s^{\sqcap}((k-d_2)\delta_r, \tau_2)^*\right] \\ &\qquad \cdot e^{j2\pi\delta_t(d_2\tau_2 - d_1\tau_1)} d\tau_1 d\tau_2. \end{aligned} \tag{D.2}$$

By (12) it is readily apparent that

$$\begin{aligned} &\mathrm{E}\left[s^{\sqcap}((k-d_1)\delta_r, \tau_1) s^{\sqcap}((k-d_2)\delta_r, \tau_2)^*\right] \\ &\quad = \mathrm{sinc}(fN_s(T + \Delta T))^2 * S_{ss}(f, \tau)\Big|_{f=(k-d)\delta_r} \\ &\qquad \cdot N_s^2(T + \Delta T)^2 \delta_{d_1 d_2} \delta(\tau_2 - \tau_1), \end{aligned} \tag{D.3}$$

where δ_{pq} is the Kronecker delta. Given (13) and (15) and our assumption that the data symbols are uncorrelated with average energy E_s, we can simplify (D.2) to obtain

$$\mathrm{E}[I(k)I^*(k)] = E_s \sum_{\substack{d=-N_s/2 \\ d\neq k}}^{N_s/2-1} \beta(d,d)\beta^*(d,d) S^{\sqcap}((k-d)\delta_r). \tag{D.4}$$

Similarly, for $\varphi(k)$,

$$\begin{aligned} &\mathrm{E}[\varphi(k)\varphi^*(k)] \\ &\quad = \frac{1}{N_s^2(T + \Delta T)^2} \sum_{d_1=-N_s/2}^{N_s/2-1} \sum_{\substack{\nu_1=-N_s/2 \\ \nu\neq d_1}}^{N_s/2-1} \sum_{d_2=-N_s/2}^{N_s/2-1} \sum_{\substack{\nu_2=-N_s/2 \\ \nu_2\neq d_2}}^{N_s/2-1} \\ &\qquad \cdot \mathrm{E}[X_m(\nu_1)X_m^*(\nu_2)]\beta(d_1, \nu_1)\beta^*(d_2, \nu_2) \\ &\qquad \cdot \iint_0^\infty \mathrm{E}\left[s^{\sqcap}((k-d_1)\delta_r, \tau_1) s^{\sqcap}((k-d_2)\delta_r, \tau_2)^*\right] \\ &\qquad \cdot e^{j2\pi\delta_t(\nu_2\tau_2 - \nu_1\tau_1)} d\tau_1 d\tau_2. \end{aligned} \tag{D.5}$$

Using again (D.3) and uncorrelated data symbols we get

$$\mathrm{E}[\varphi(k)\varphi^*(k)] = E_s \sum_{d=-N_s/2}^{N_s/2-1} \sum_{\substack{\nu=-N_s/2 \\ \nu\neq d}}^{N_s/2-1} S^{\sqcap}((k-d)\delta_r)\beta(d,\nu)\beta^*(d,\nu). \tag{D.6}$$

Equations (18) and (19) are obtained by separating the term for $d = k$ from the rest of the sum on d in (D.6).

Finally, the cross-correlations are

$$\begin{aligned}\mathrm{E}[I(k)\varphi^*(k)] &= \frac{1}{N_s^2(T+\Delta T)^2} \sum_{\substack{d_1=-N_s/2 \\ d_1\neq k}}^{N_s/2-1} \sum_{d_2=-N_s/2}^{N_s/2-1} \sum_{\substack{\nu_2=-N_s/2 \\ \nu_2\neq d_2}}^{N_s/2-1} \\ &\quad \cdot \mathrm{E}[X_m(d_1)X_m^*(\nu_2)]\beta(d_1,d_1)\beta^*(d_2,\nu_2) \\ &\quad \cdot \iint_0^{\infty} \mathrm{E}\left[s^{\sqcap}((k-d_1)\delta_r,\tau_1)s^{\sqcap}((k-d_2)\delta_r,\tau_2)^*\right] \\ &\quad \cdot e^{j2\pi\delta_t(\nu_2\tau_2-d_1\tau_1)}d\tau_1 d\tau_2.\end{aligned} \tag{D.7}$$

In this case, assuming uncorrelated data symbols eliminates all summands in (D.7) except those for $d_1 = d_2$ and $d_1 = \nu_2$. Then, because the sum on ν_2 leaves out the terms $\nu_2 = d_2$, we find that (D.7) equals zero.

Acknowledgment

This work was supported by Grants FONDECYT 1060718 and ADI-32 2006 from CONICYT Chile.

References

[1] H. Steendam and M. Moeneclaey, "Analysis and optimization of the performance of OFDM on frequency-selective time-selective fading channels," *IEEE Transactions on Communications*, vol. 47, no. 12, pp. 1811–1819, 1999.

[2] W. G. Jeon, K. H. Chang, and Y. S. Cho, "An equalization technique for orthogonal frequency-division multiplexing systems in time-variant multipath channels," *IEEE Transactions on Communications*, vol. 47, no. 1, pp. 27–32, 1999.

[3] Y. Li and L. J. Cimini Jr., "Bounds on the interchannel interference of OFDM in time-varying impairments," *IEEE Transactions on Communications*, vol. 49, no. 3, pp. 401–404, 2001.

[4] A. Stamoulis, S. N. Diggavi, and N. Al-Dhahir, "Intercarrier interference in MIMO OFDM," *IEEE Transactions on Signal Processing*, vol. 50, no. 10, pp. 2451–2464, 2002.

[5] A. Stamoulis, S. N. Diggavi, and N. Al-Dhahir, "Estimation of fast fading channels in OFDM," in *Proceedings of IEEE Wireless Communications and Networking Conference (WCNC '02)*, vol. 1, pp. 465–470, March 2002.

[6] Y. Mostofi and D. C. Cox, "ICI mitigation for pilot-aided OFDM mobile systems," *IEEE Transactions on Wireless Communications*, vol. 4, no. 2, pp. 765–774, 2005.

[7] K. W. Park and Y. S. Cho, "An MIMO-OFDM technique for high-speed mobile channels," *IEEE Communications Letters*, vol. 9, no. 7, pp. 604–606, 2005.

[8] D. Huang, K. B. Letaief, and J. Lu, "Bit-interleaved time-frequency coded modulation for OFDM systems over time-varying channels," *IEEE Transactions on Communications*, vol. 53, no. 7, pp. 1191–1199, 2005.

[9] W.-S. Hou and B.-S. Chen, "ICI cancellation for OFDM communication systems in time-varying multipath fading channels," *IEEE Transactions on Wireless Communications*, vol. 4, no. 5, pp. 2100–2110, 2005.

[10] P. H. Moose, "A technique for orthogonal frequency division multiplexing frequency offset correction," *IEEE Transactions on Communications*, vol. 42, no. 10, pp. 2908–2914, 1994.

[11] T. Pollet, M. van Bladel, and M. Moeneclaey, "BER sensitivity of OFDM systems to carrier frequency offset and Wiener phase noise," *IEEE Transactions on Communications*, vol. 43, no. 2, pp. 191–193, 1995.

[12] J. Armstrong, "Analysis of new and existing methods of reducing intercarrier interference due to carrier frequency offset in OFDM," *IEEE Transactions on Communications*, vol. 47, no. 3, pp. 365–369, 1999.

[13] T. Keller, L. Piazzo, P. Mandarini, and L. Hanzo, "Orthogonal frequency division multiplex synchronization techniques for frequency-selective fading channels," *IEEE Journal on Selected Areas in Communications*, vol. 19, no. 6, pp. 999–1008, 2001.

[14] Y. Zhao and S.-G. Häggman, "Intercarrier interference self-cancellation scheme for OFDM mobile communication systems," *IEEE Transactions on Communications*, vol. 49, no. 7, pp. 1185–1191, 2001.

[15] K. Sathananthan and C. Tellambura, "Probability of error calculation of OFDM systems with frequency offset," *IEEE Transactions on Communications*, vol. 49, no. 11, pp. 1884–1888, 2001.

[16] T. Pollet, P. Spruyt, and M. Moeneclaey, "The BER performance of OFDM systems using non-synchronize sampling," in *Proceedings of IEEE Global Telecommunications Conference (GLOBECOM '94)*, vol. 1, pp. 253–257, San Francisco, Calif, USA, November-December 1994.

[17] M. Speth, S. A. Fechtel, G. Fock, and H. Meyr, "Optimum receiver design for wireless broad-band systems using OFDM—part I," *IEEE Transactions on Communications*, vol. 47, no. 11, pp. 1668–1677, 1999.

[18] F. Horlin, S. De Rore, E. Lopez-Estraviz, F. Naessens, and L. van der Perre, "Impact of frequency offsets and IQ imbalance on MC-CDMA reception based on channel tracking," in *Proceedings of the 8th International Symposium on Wireless Personal Multimedia Communications (WPMC '05)*, Aalborg, Denmark, September 2005.

[19] C. Oberli, "ML-based tracking algorithms for MIMO-OFDM," *IEEE Transactions on Wireless Communications*, vol. 6, no. 7, pp. 2630–2639, 2007.

[20] J. Li and M. Kavehrad, "Effects of time selective multipath fading on OFDM systems for broadband mobile applications," *IEEE Communications Letters*, vol. 3, no. 12, pp. 332–334, 1999.

[21] IEEE Std. 802.16e-2005, "Part 16: Air Interface for Fixed and Mobile Broadband Wireless Access Systems—Ammendment 2: Physical and Medium Access Control Layers for Combined Fixed and Mobile Operation in Licensed Bands and Corrigendum 1," http://standards.ieee.org/getieee802.

[22] P. Bello, "Characterization of randomly time-variant linear channels," *IEEE Transactions on Communications*, vol. 11, no. 4, pp. 360–393, 1963.

[23] M. Pätzold, *Mobile Fading Channels*, John Wiley & Sons, New York, NY, USA, 2002.

[24] ETSI Std. EN 300 744 V1.5.1, "Digital Video Broadcasting (DVB); Framing structure, channel coding and modulation for digital terrestrial television," June 2004.

[25] M. Russell and G. L. Stuber, "Interchannel interference analysis of OFDM in a mobile environment," in *Proceedings of the 45th IEEE Vehicular Technology Conference (VTC '95)*, vol. 2, pp. 820–824, Chicago, Ill, USA, July 1995.

[26] R. Clarke, "A statistical theory of mobile radio reception," *The Bell System Technical Journal*, vol. 47, pp. 957–1000, 1968.

[27] M. García, *A general model for intercarrier interference in OFDM*, M.S. thesis, Pontificia Universidad Católica de Chile, Santiago, Chile, May 2008.

[28] K. E. Baddour and N. C. Beaulieu, "Autoregressive modeling for fading channel simulation," *IEEE Transactions on Wireless Communications*, vol. 4, no. 4, pp. 1650–1662, 2005.

[29] T. S. Rappaport, *Wireless Communications: Principles & Practice*, Prentice-Hall, Upper Saddle River, NJ, USA, 2nd edition, 2002.